Supporting Information

A green catalyst and sensor: Band engineering of $Bi_2Fe_4O_9$ based S-scheme p-n/n homo-heterojunction for detection and degradation of cytotoxic drug

Deepeka[a], Jyoti[a], Paramdeep kaur[a], Komal[a], Sandeep Bansal[b], Vinod Kumar[c], Kulbhushan Tikoo[c] and Sonal Singhal[a]*

[a]Department of Chemistry, Panjab University, Chandigarh, 160014, India.

[b]Department of Science and Technology, New Delhi, India.

[c]HR-TEM Facility Lab Department of Pharmacology and Toxicology, National Institute of Pharmaceutical Education and Research (NIPER), SAS Nagar-160062, Punjab, India.

*sonal1174@gmail.com ; sonal@pu.ac.in

CORRESPONDING AUTHOR:

Sonal Singhal
Professor,
Department of Chemistry,
Chandigarh
Ph. No. +91-172-2534421(o)
+91-09872118810(m)
E-mail: sonal1174@gmail.com

Table of content

List of Figures

Fig. S7 *Deconvoluted XPS spectra of (a) Bi 4f, (b) Fe 2p, (c) O 1s of BF and (d) C 1s (inset showing the survey scan of AFTS), (e) Ca 2p, (f) O 1s and (g) N 1s of AFTS.*

Fig. S8 *Control experiments (a) for the degradation of LF using BF AF50TS as catalyst at pH 2.5, (b) degradation of pollutants at neutral pH using BF AF50TS in presence of light (without oxidant).*

Fig. S9 *Time dependent % removal plots showing the photocatalytic degradation of (a) DR and (b) LF using BF and p-n/n homo-heterojunction.*

Fig. S10 *Pseudo first order kinetic curves for the photocatalytic degradation of DR and LF using BF and p-n/n homo-heterojunctions.*

Fig. S11 *Pseudo first order kinetic curves for the catalytic degradation (without light irradiation) of DR and LF using BF and p-n/n homo-heterojunction.*

Fig. S12 *(a) Radical scavenging studies of LF using BF AF50TS as catalyst, (b) % Removal plots revealing the optimized catalyst loading.*

Fig. S13 *GC-MS fragment analysis chart for DR intermediates in presence of light only.*

Fig. S14 *GC-MS fragment analysis chart for DR intermediates in presence of oxidant, BF 50AFTS and light.*

Fig. 15 *(a) Interference of possible anions on %removal of DR (b) leaching of metal ions during degradation of DR utilizing BF an BF 50AFTS (catalyst amount used 0.60 g/L and pH = 2.5)*

Fig. S16 *(a) % Removal of TOC using BF and BF 50AFTS, (b) Time-dependent UV–visible spectra for degradation of mixture of SO, RB-Y, DR and LF using BF 50AFTS p-n/n homo-heterojunction , (c) Recyclability studies of BF 50AFTS.*

Fig. S17 *(a, b) FE-SEM image at 1 mm and 400 nm, and (c) TEM image at 100 nm of recovered BF 50AFTS.*

Fig. S18 *SWASV response of BF 50AFTS@GCE for DR (a) at different pH in acetate buffer (b) with varying accumulation potential (c) for different accumulation times.*

Fig. S19 *Interference studies for various drugs (levofloxacin (LF), ofloxacin (OF), ciprofloxacin (CF), tetracycline (TC), diclofenac (DF), paracetamol (PCM)), ascorbic acid (AA), uric acid (UA), glucose (GL), dopamine (DA) and nitro phenols (2-aminophenol (2AP)*

and 4-aminophenol (2AP)) on detection of 17.27 μM of DR in 0.1 M acetate buffer (pH = 5.0)

Fig. S20 *(a) Current response obtained for 17.27 μM DR drug obtained from repeatability analysis of BF 50AFTS@GCE and (b) Reproducibility analysis of BF 50AFTS@GCE with 17.27 μM DR under optimized parameters.*

List of tables

102 **Synthesis method**

103 BF (x wt%)TS (x= 0, 25, 50, 75) p-n/n homo-heterojunction were synthesised via well-
104 known hydrothermal route. Equimolar amounts of $Bi(NO_3)_3.5H_2O$ and $FeCl_3.6H_2O$ were
105 dissolved in 500 mL distilled water containing 100 mL acetone. pH of the solution was adjusted
106 in the range of 10-11 by adding ammonia solution, thick brown precipitates were obtained.
107 Precipitates were washed with distilled water several times till neutral pH was attained. The
108 precipitates were separated out via centrifugation and dispersed in aqueous sodium hydroxide
109 solution followed by addition of varying amount of TS powder (before use TS were washed,
110 grounded and sieved). The obtained mixture was then transferred to Teflon autoclave and kept
111 in a preheated hot air oven at constant temperature of 140 ºC for 72 h. Final product was washed
112 with distilled water and ethanol followed by drying at 70 ºC for 16 h [17]. Pristine BF
113 nanoplates were also synthesised using the above mentioned method, without addition of TS
114 powder.

115 Further, amination reaction was performed to modify TS powder with amine
116 functionalities [2]. For this, 2 g of TS powder was dispersed in 400 mL of 1 M NaOH under
117 ultrasonication followed by magnetic stirring. 18 mmol epichlorohydrin was added to the
118 mixture and allowed to react for 2 h at 60 ºC. In order to attain pH below 12, the mixture was
119 washed repeatedly with deionized water. Treated powder was recovered via centrifugation and
120 further treated with sodium hydroxide (400 mL, 0.1 M) and ammonia solution (15 mL, 29.4%
121 w/v) for another 2 h at 60 ºC. Final product was washed several times with water till neutral
122 was attained and dried at 45 ºC in hot air oven. The aminated TS powder was then utilized for
123 synthesis of BF 50AFTS as mentioned above.

124 **Catalytic Procedure**

125 100 mL model pollutant solution of DR and LF (50 mg/L) was introduced with 60 mg
126 synthesized catalyst and dispersed under ultrasonication for 5 min. Obtained solution was kept
127 in dark under magnetic stirring for 30 min to attain the needful adsorption-desorption
128 equilibrium (100-120 rpm). 100 mL of H_2O_2 (8.8 mM, 30% w/v) was added to the solution
129 followed by stirring (100-120 rpm) under visible light irradiation (400 W Hg lamp operating
130 at 220 V as visible light source with light intensity near the surface of solution to be
131 51.2 mW/cm^2). Small sample aliquots were withdrawn at fixed time intervals and catalyst was

separated via centrifugation, obtained supernatant was then analyzed with UV-vis spectrophotometer.[3]

Phytotoxicity assessment procedure

After sanitization, selected healthy and uniform sized mung seeds (*Vigna radiata*) were swamped (for 3 h) in the river water containing 0.5 mg/mL BF 50AFTS. After 3 h seeds were stained out and kept undisturbed for 5 days under moist conditions. Similar experiments were performed for blank river water and river water containing contamination (DR and LF before phototreatment and after phototreatment). In order to maintain the integrity all experiments were performed thrice and after 5 days mean root elongation (MRE in cm) of seedlings was measured. Further, GP (germination %,) using equation S1 and SVI (seedling vigour index) using equation S2 were also calculated to measure the Phytotoxicity.[4]

$$GP = \frac{Germinated\ seeds}{Total\ number\ of\ seeds} * 100 \quad \text{(S1)}$$

$$SVI = GP * Avrage\ length\ of\ seedling \quad \text{(S2)}$$

Fabrication of electrode

The Glassy carbon electrode (GCE) was cleaned properly using alpha-alumina Powder slurry (0.5 μm). GCE was then sonicated (for 60 second in ethanol and water) and dried at room temperature. A uniform dispersion of catalyst (5 mg/mL) was prepared in aqueous medium, 4 μL suspension was robbed to drop casted on prewashed GCE and allowed to dry naturally. To study sensing ability of modified electrode towards DR drug cyclic voltammetric and square wave anodic stripping voltammetric studies were performed in acetate buffer (supporting electrolyte) having pH 5.

Characterization techniques

The instrumental details for characterization studies performed in the current work are: Structural features and presence of functional groups were assessed utilizing Fourier Transform Infrared spectra in the range of 450 to 4000 cm-1 (Nicolet iS50 FT-IR) , Phase purity and crystal structure were examined using X-ray diffractometer (Panalytical's X'Pert Pro diffractometer) with CuKα radiation (λ = 1.5406 Å). Field Emission Scanning Electron Microscopy (FE-SEM, Hitachi- SU8010) and High Resolution- Transmission Electron Microscope (HR-TEM, FEI Tecnai (G2 F20) operating at 200 keV) were utilized to ascertain morphological and elemental composition studies. Elemental oxidation states were examined

using X-ray Photoelectron Spectroscopy (XPS) Nexsa Base, (Thermofisher Scientific), JASCO, V- 750; UV–Vis Spectrophotometer was employed to investigate optical and degradation studies. Thermo Scientific TSQ 8000 GC-MS (instrument method - Solvent Delay_4.5m) was utilized to ascertain intermediates and by-products generated during degradation. Photoluminescence studies were performed using Hitachi Fluorescence Spectrophotometer (F- 7000), Photo-irradiation was braced by 400 W Hg lamp operating at 220 V, BrunauereEmmetteTeller (BET, Belsorp max) was employed for surface area studies and Raman analysis was performed using HORIBA JAPAN Xplor PLUS instrument. STD Q600 TA instrument was utilized to testify thermal stability of synthesised materials. iCAP-RQ ICP-MS (Inductive Coupled Plasma Mass Spectroscopy) was employed for quantification of metal ion leaching. Electrochemical studies were performed using Metrohm Autolab/PGSTAT204 electrochemical work station. Atomic force microscopy using AFM

Fourier Transform Infrared (FT-IR)

The detailed information regarding structural changes and presence of functional groups on RTS (raw tamarind shell), BF (x)TS (x= 25, 50, 75 wt%) and BF 50AFTS was congregated via FT-IR spectroscopy (Fig. S1 (a)). In case of $Bi_2Fe_4O_9$, four iron atoms have two different sites, $Fe_{(a)}$ occupies a tetrahedral site, while $Fe_{(b)}$ having octahedral site. The bands at ~ 442 and 491 cm^{-1} could be attributed to stretching and bending vibrations of Fe-O in octahedral coordination of BF. Whereas, the band arising at ~ 807 and 628 cm^{-1} may be due to tetrahedral stretching vibrations of Fe-O in tetrahedral coordination.[5] In case of RTS, presence of hydroxyl (~ 3400 cm^{-1}), carboxyl (1730 cm^{-1}), amine (1520 cm^{-1}) and ester (1740 cm^{-1}) groups were observed by FT-IR spectra (Fig. S1 (a)), bands roused at ~ 1048 and 1630 cm^{-1} indicated the presence of stretching vibrations of C-O and CH_2=CH_2, respectively. The weak bands present at ~2920 and 2850 cm^{-1} were assigned to stretching vibrations of -CH_2- and -CH- bonds of methylene groups, respectively. The band with decent intensity at ~ 1440 cm^{-1} confirmed the presence of C=C stretch of aromatic rings; but in case of FT-IR spectra of BF (x)TS p-n/n homo-heterojunction, the band at ~1440 (corresponding to C=C stretch) and two other bands at ~1520 and 1740 cm^{-1} (corresponding to amine and ester groups) get vanished indicating the removal of some C=C stretching vibrations, amine and ester groups, respectively. Reduction of TS powder in presence of NaOH and high temperature during synthesis could be the possible reason for this observation. This reduction produced additional binding sites and free electrons, beneficial for catalytic reactions.[6] In case of BF 50AFTS, extensive broadening in FTIR band at ~ 3440 cm^{-1} along with shoulder (overtone of N-H

bending vibrations) at ~ 3250 cm^{-1} confirmed the presence of N-H stretching of amine group. Weak bands around ~ 1500 and 710 cm^{-1} indicates the presence of C-N bending and N-H wagging vibrations of amine, respectively, confirming the presence of amine functionalize TS in the p-n/n homo-heterojunction.[7] Thus, it can be concluded that the natural amine groups of TS could not survive under current reaction conditions. But amine group provided by amination reaction lasted long even at high temperature conditions.

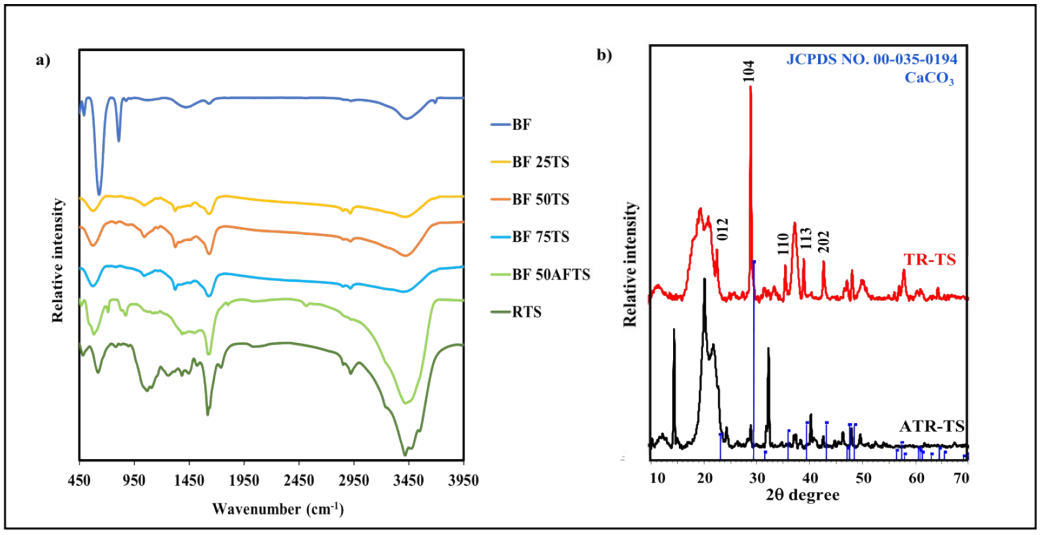

Fig. S1 (a) FT-IR spectra of RTS, BF and synthesized p-n/n homo-heterojunction and (b) PXRD spectra of hydrothermally treated TS powder.

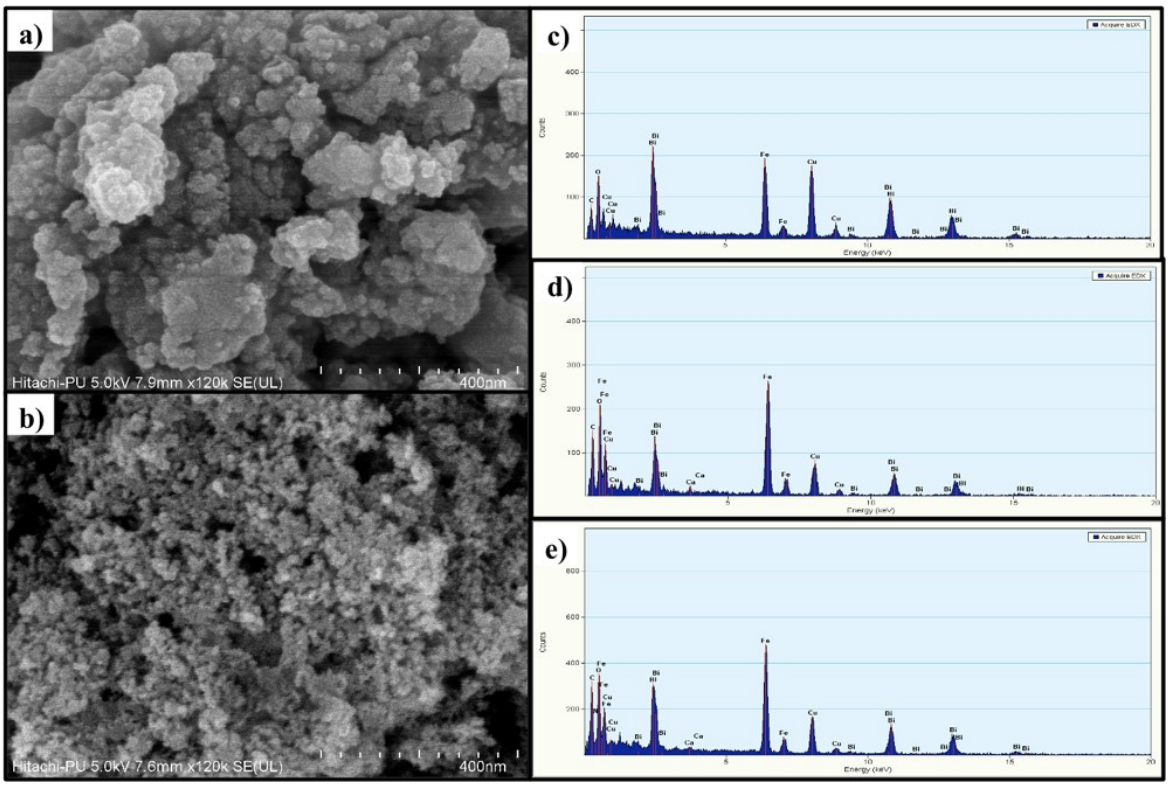

Fig. S2 FE-SEM micrographs of (a) treated TS powder and (b) treated AFTS powder, EDX spectra of (c) BF, (d) BF 50TS and (e) BF 50AFTS.

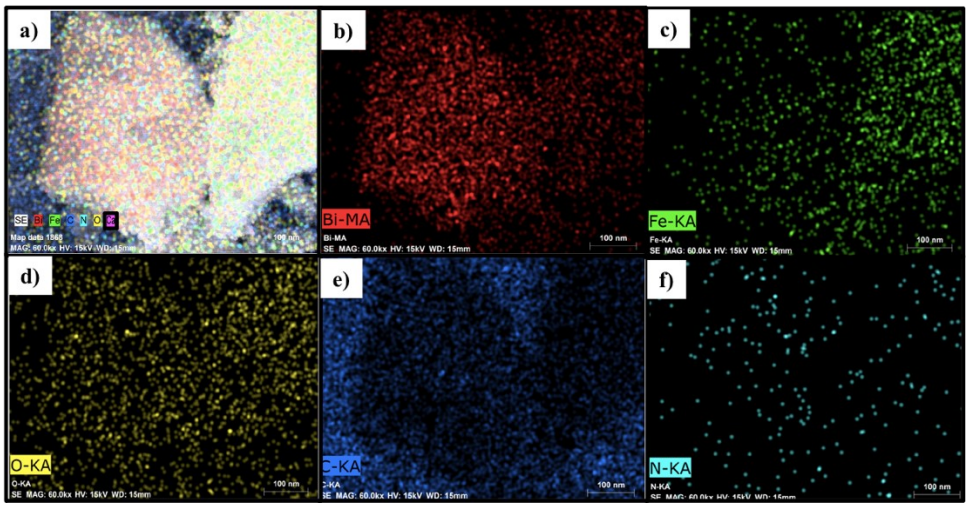

Fig. S3. Mapping image of BF 50AFTS.

Raman Spectroscopy

Raman spectra of BF and composites (BF 50TS and BF 50AFTS) were recorded using 200 μm slit and presented in Fig. S4.

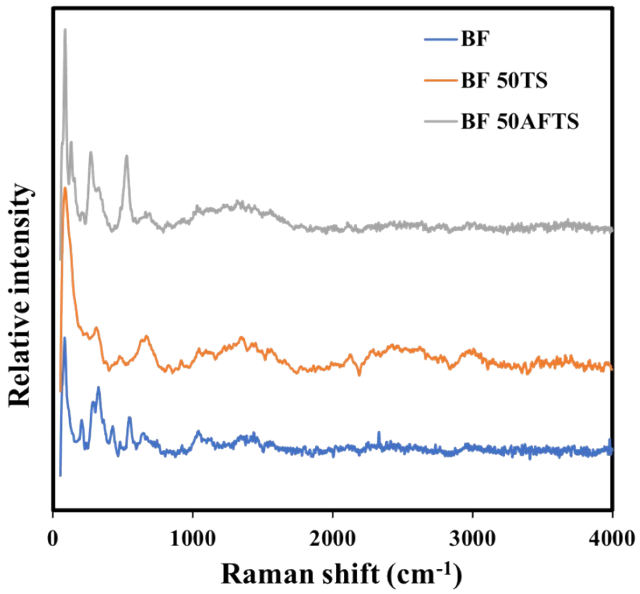

Fig. S4 Raman spectra of BF and p-n/n homo-heterojunction.

The orthorhombic bismuth ferrite possess 42 active modes of Raman ($12A_g + 12B_{1g} + 9B_{2g} + 9B_{3g}$) out of which 10 modes were observed here at 80, 126, 210, 305, 340, 400, 470, 540, 625, 698 cm^{-1}.[8] The Raman modes below 170 cm^{-1} could be attributed to A_g mode of Bi atoms that vibrates along the x-y plane. The Raman modes existing in the range of 150-250 cm^{-1} represent A_g mode generated from vibrations of Fe atoms along the X-Y plane. Furthermore, the Raman modes above 250 cm^{-1} aroused due to stretching motion of oxygen.[9] Presence of broad hump in the range of 900 - 1700 cm^{-1} corresponding to G and D bands certified the presence of carbonaceous material in case of BF 50TS and BF 50AFTS, thereby confirming the successful fabrication of p-n/n homo-heterojunctions.

Table. S1 Values of crystallite size (D), lattice parameters (a, b, c) and band gap (E_g) for synthesized BF and p-n/n homo-heterojunction.

Catalyst	a (Å)	b (Å)	c (Å)	Crystallite size (nm)	Band gap (eV)
BF	7.962	8.471	6.014	42.9	2.19
BF 25TS	8.044	8.803	6.102	41.1	2.05
BF 50TS	7.872	8.364	5.983	39.9	1.93
BF 75TS	7.861	8.353	5.954	35.2	2.01

BF 50AFTS	7.874	8.352	5.972	39.7	1.91
AFTS	-	-	-	-	2.04

Table S2 Elemental composition of BF, BF 50TS and BF 50AFTS.

Elements	Weight% BF	Atomic% BF	Weight% BF 50FTS	Atomic% BF 50FTS	Weight% BF 50AFTS	Atomic% BF 50FTS
C(K)	-	-	17.70	48.56	18.57	51.40
O(K)	11.98	50.55	13.26	27.30	11.44	23.77
Ca(K)	-	-	1.10	0.05	0.25	0.21
Fe(K)	23.73	28.68	28.93	17.06	25.40	15.11
Bi(L)	64.27	20.75	38.98	6.14	43.22	6.87
N(K)	-	-	-	-	1.09	2.60

Brunauer-Emmett-Teller (BET) Surface Area Studies

Catalytic ablity of a material highly depends on its surface area, in this concern N_2 adsorption/desorption (Brunauer-Emmett-Teller) analysis was accomplished to appraise the specific surface area and porous characteristics of the synthesized nanomaterials. Prior to adsorption of N_2 on surface of nanomaterials, degassing process was carried out at 100 ºC for 1h. After analyzing the relative pressure of gas, amount of gas adsorbed was examined and values of specific surface area were calculated using BET adsorption equation. The typical linear plots of $1/[Q\{(P_O/P)-1\}]$ *vs.* relative pressure for BF, BF 50TS and BF 50AFTS are depicted in Fig. S5. The results analysed from graph were interpreted utilizing the mathematical formula presented by earlier literature reports.[10, 11] The specific surface area value for BF was found to be 4.32 m^2/g, while dramatical enhancement in surface area was observed with introduction of 50% TSP and much larger values of surface area 43.4 m^2/g was obtained for BF 50TS i.e., 10 fold enhancement was observed with introduction of 50 wt% TS. The significantly large value of surface area of BF 50TS as that of BF could be attributed to highly porous and extremely small particles of TS. Furthermore, BF 50AFTS posed

phenomenally high value of surface area (99.0 m^2/g), i.e. amination reaction of TS led to approximately two fold enhancement of surface area. The dramatical hike in surface area with implantation of amine functionalities could be the result of decrease in aggregation between AFTS particles (as that of TS) as reviled by FE-SEM studies (Fig. S2 (a, b)).

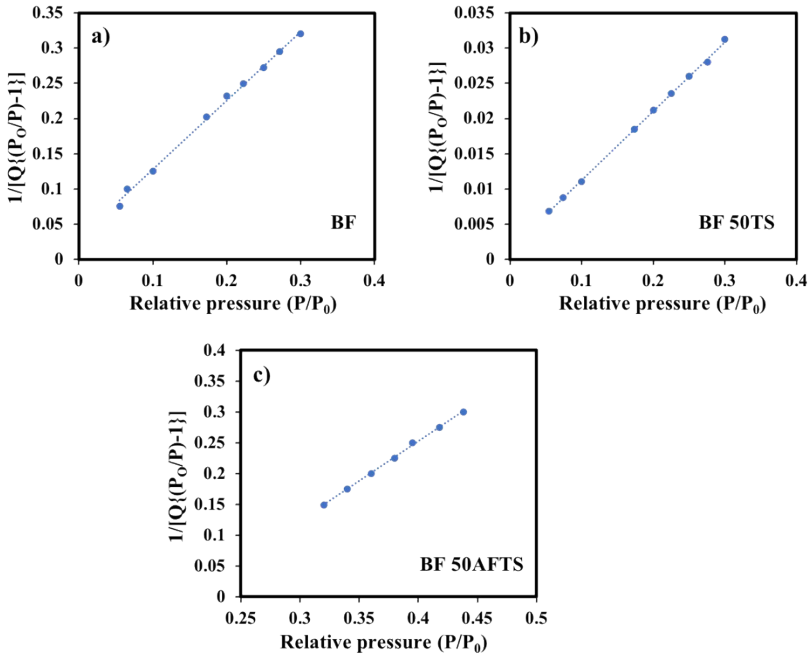

Fig. S5 BET linear plots of (a) BF nanoplates, (b) BF 50TS and (c) BF 50AFTS.

Thermogravimetric Analysis (TGA)

Thermal stability of material was testified upto 1000 ºC under TGA analysis, BF plates were found to be highly stable upto 1000 ºC (Fig. S6 (b)). Only 5.9% weight loss was observed for BF, evaporation of residual water molecules could be the possible reason for the weight loss. While in case of BF 50TS and BF 50AFTS, ~ 38% weight loss was observed upto 1000 ºC, additional weight loss of 32% in case of p-n/n homo-heterojunction may be due to the decomposition of some carbon content. From TGA curves of both the p-n/n homo-heterojunction, it can be clearly seen that weight loss in BF 50AFTS is more as that of BF 50TS, which may be due to the decomposition of slightly high concentration of water content (i.e. 4% weight loss difference below 200 ºC) and some organic compounds used during amination process. It can be concluded that some part (~ 18%) of the carbonaceous material (fabricated from TSP) present in p-n/n homo-heterojunction is highly stable.

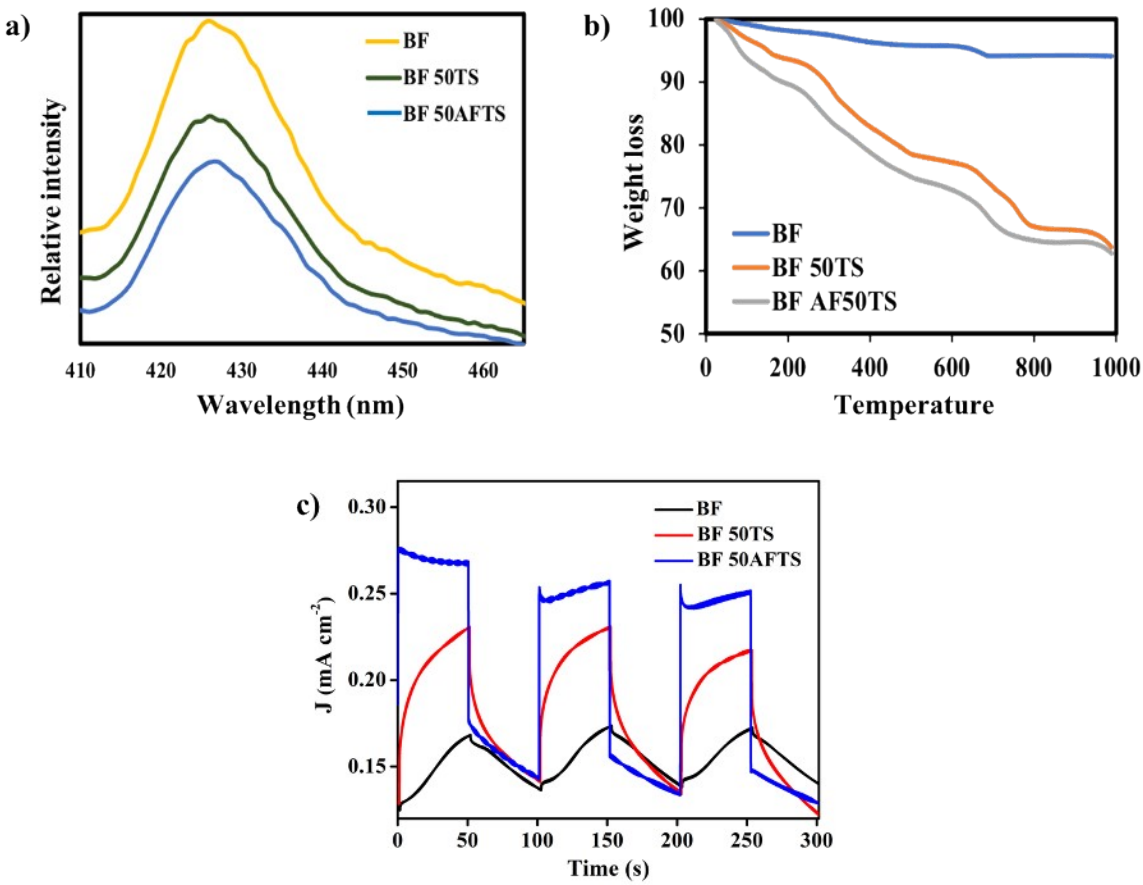

Fig. S6 (a) PL spectra and (b) thermogravimetric analysis curves (c) Photocurrent response of BF, BF 50TS and BF 50AFTS.

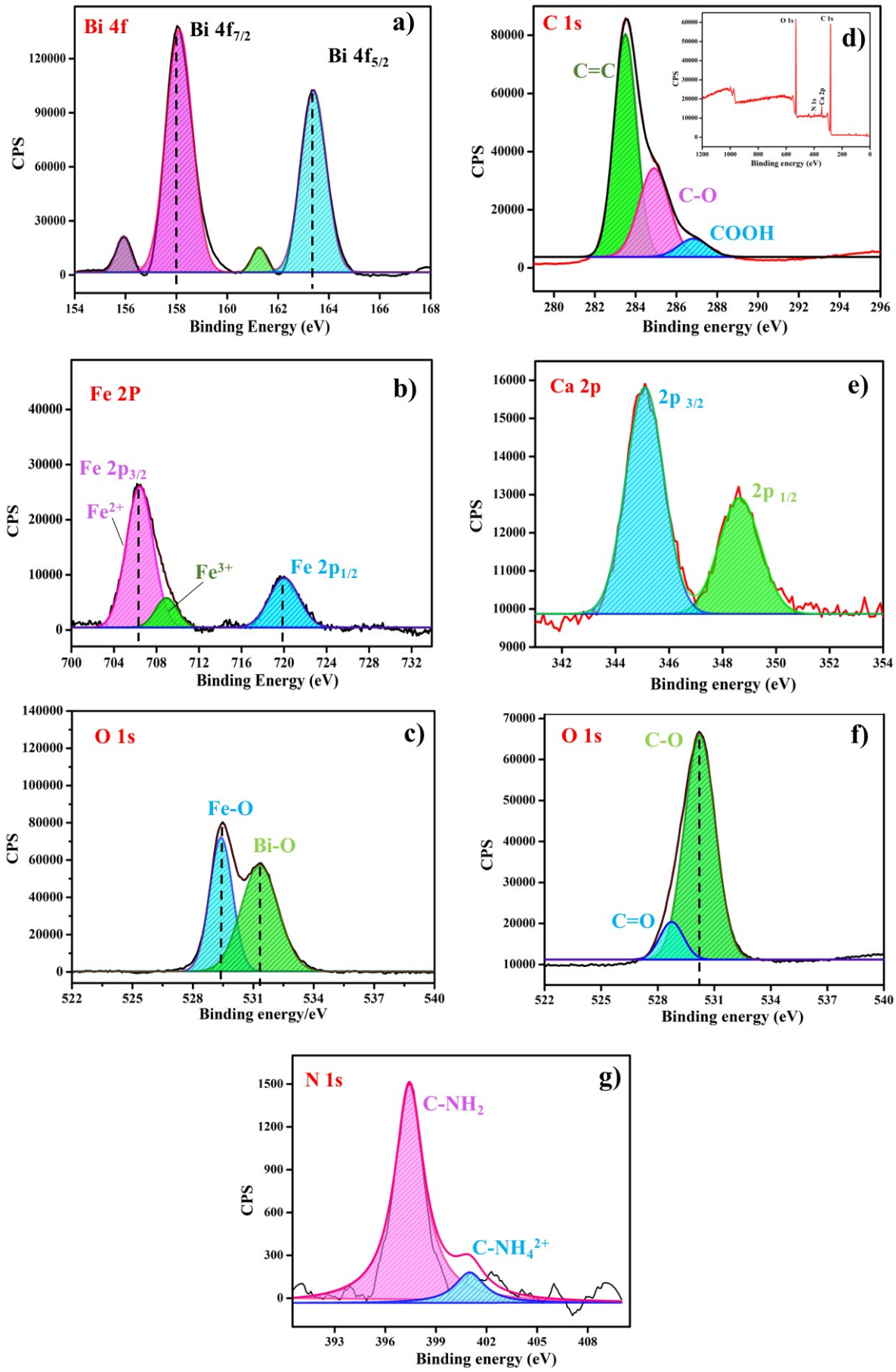
Bi 4f
a)
Bi 4f7/2
Bi 4f5/2
CPS
Binding Energy (eV)
C 1s
d)
C=C
C-O
COOH
O 1s
N 1s
Ca 2p
Binding energy (eV)
Fe 2P
b)
Fe 2p3/2
Fe2+
Fe3+
Fe 2p1/2
Binding Energy (eV)
Ca 2p
e)
2p 3/2
2p 1/2
Binding energy (eV)
O 1s
c)
Fe-O
Bi-O
Binding energy/eV
O 1s
f)
C-O
C=O
Binding energy (eV)
N 1s
g)
C-NH2
C-NH4 2+
Binding energy (eV)

266

Fig. S7 Deconvoluted XPS spectra of (a) Bi 4f, (b) Fe 2p, (c) O 1s of BF and (d) C 1s (inset showing the survey scan of AFTS), (e) Ca 2p, (f) O 1s and (g) N 1s of AFTS.

Optimization of reaction constraints

In order to investigate the necessary conditions for oxidative degradation of model pollutants, control experiments and optimization studies were performed for LF drug utilizing the BF 50TS as catalyst. Various reaction constraints such as oxidant, catalyst and light were examined at pH 2.5 using BF AF50TS as catalyst as shown in Fig. S8 (a). The synthesized catalyst was found to be highly efficient even in the absence of light whereas, best results were obtained when ferrite + catalyst + oxidant + light were present all together. Fig. S8 (b) showcased efficiency of synthesized BF AF50TS for degradation of model pollutants in absence of acid and oxidant (i.e. in presence of catalyst and light only), more than 67% removal was observed for all the model pollutants. 95% removal of DR and 67% removal of LF (in 120 min) even in absence of acid and oxidant showcased appreciable efficacy of synthesized material.

The catalyst Dosage was varied from 0.30 to 1.2 g/L and the rate of reaction was observed to increase with amount of catalyst up to 0.60 g/L and further increase in catalyst dosage exhibited a slight increase in catalytic activity which could be due to saturation of surface active sites hence, 0.60 g/L was considered as the optimal catalytic dosage for further reactions (Fig. S12 (b)).

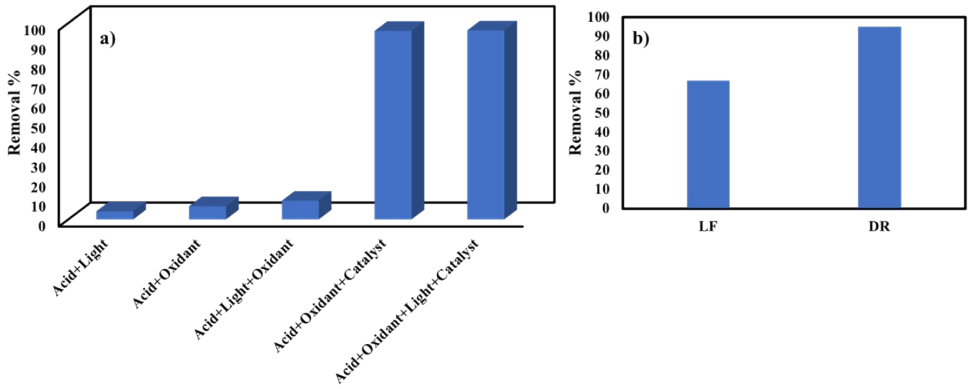

Fig. S8 Control experiments for the degradation of LF (a) under different reaction conditions using BF AF50TS as catalyst at pH 2.5, (b) at neutral pH using BF AF50TS in presence of light (without oxidant).

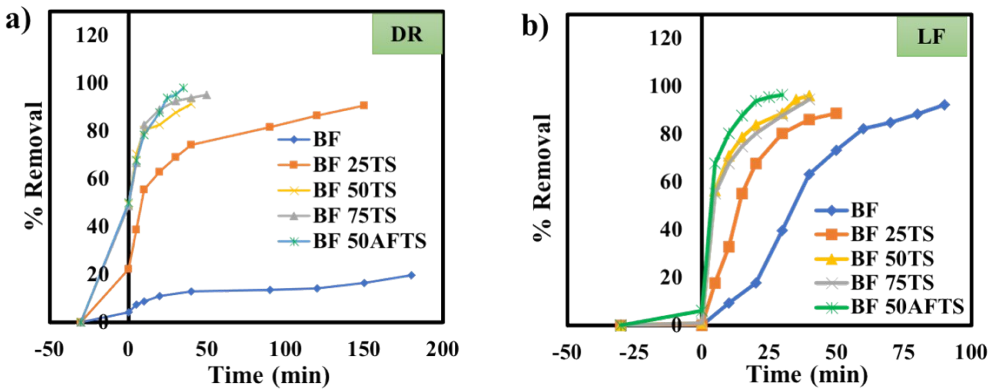

Fig. S9 Time dependent % removal plots showing the photocatalytic degradation of (a) DR and (b) LF using BF and p-n/n homo-heterojunctions.

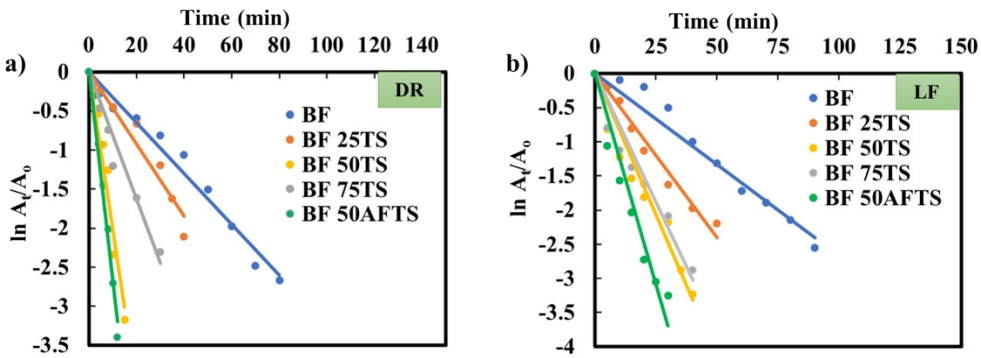

Fig. S10 Pseudo first order kinetic curves for the photocatalytic degradation of DR and LF using BF and p-n/n homo-heterojunction.

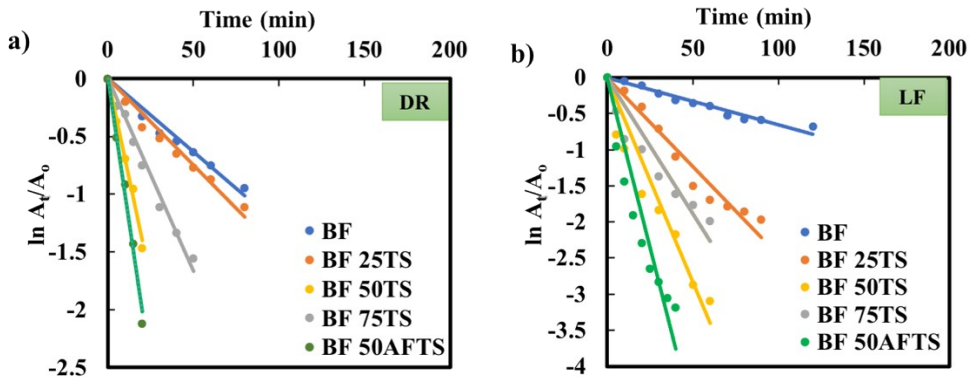

Fig. S11 Pseudo first order kinetic curves for the catalytic degradation (without light irradiation) of DR and LF using BF and p-n/n homo-heterojunctions.

Table S3 Percentage degradation, completion time and their corresponding rate constant values for the degradation of DR, LF drugs using BF and its p-n/n homo-heterojunction (with light (L) and without light (W.L)).

Catalyst	DR (W.L)		LF (W.L)	
	$k*10^{-2}$ (min^{-1})	Removal time (min) (removal %)	$k*10^{-2}$ (min^{-1})	Removal time (min) (removal%)
BF	1.2	80(62.3)	0.6	120(49.7)
BF 25TS	1.5	80(70.2)	2.4	90(88.8)
BF 50TS	6.9	20(91.8)	5.6	60(95.5)
BF 75TS	3.3	50(89.1)	3.7	60(86.5)
BF 50AFTS	**10.0**	**20(95.9)**	**9.3**	**40(96.0)**
Catalyst	**DR (L)**		**LF (L)**	
BF	3.2	80(93.2)	2.6	90(92.1)
BF 25TS	4.6	40(89.2)	4.8	50(86.6)
BF 50TS	20.0	15(99.6)	8.2	40(96.0)
BF 75TS	8.1	30(94.55)	7.5	40(94.4)
BF 50AFTS	**26.6**	**12(98.6)**	**12.2**	**30(96.3)**

Table S4. Comparison of specific photocatalytic efficiency of BF and modified BF for degradation of DR and LF.

Photocatalyst	S_{BET} (m^2/g^{-1})	Specific catalytic efficiency for degradation k/S_{BET} ($g\ m^{-2}/min$)	
		DR	LF
BF	4.32	$0.74*10^{-2}$	$0.60*10^{-2}$
BF 25TS	27.42	$0.16*10^{-2}$	$0.17*10^{-2}$

BF 50TS	43.40	$0.46*10^{-2}$	$0.18*10^{-2}$
BF 75TS	58.90	$0.13*10^{-2}$	$0.12*10^{-2}$
BF 50AFTS	99.0	$0.26*10^{-2}$	$0.12*10^{-2}$

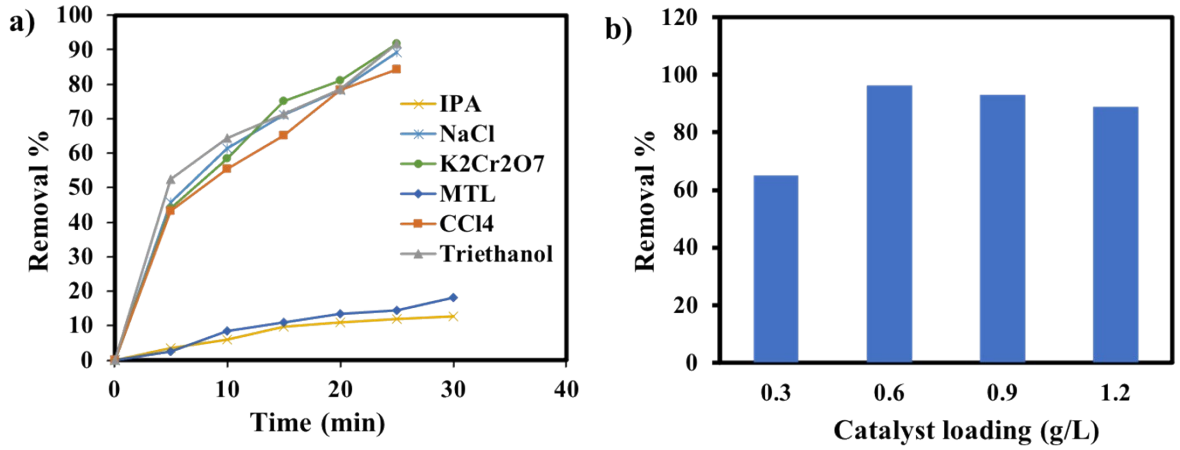

Fig. S12 (a) Radical scavenging studies of LF using BF AF50TS as catalyst, (b) % Removal plots revealing the optimized catalyst loading.

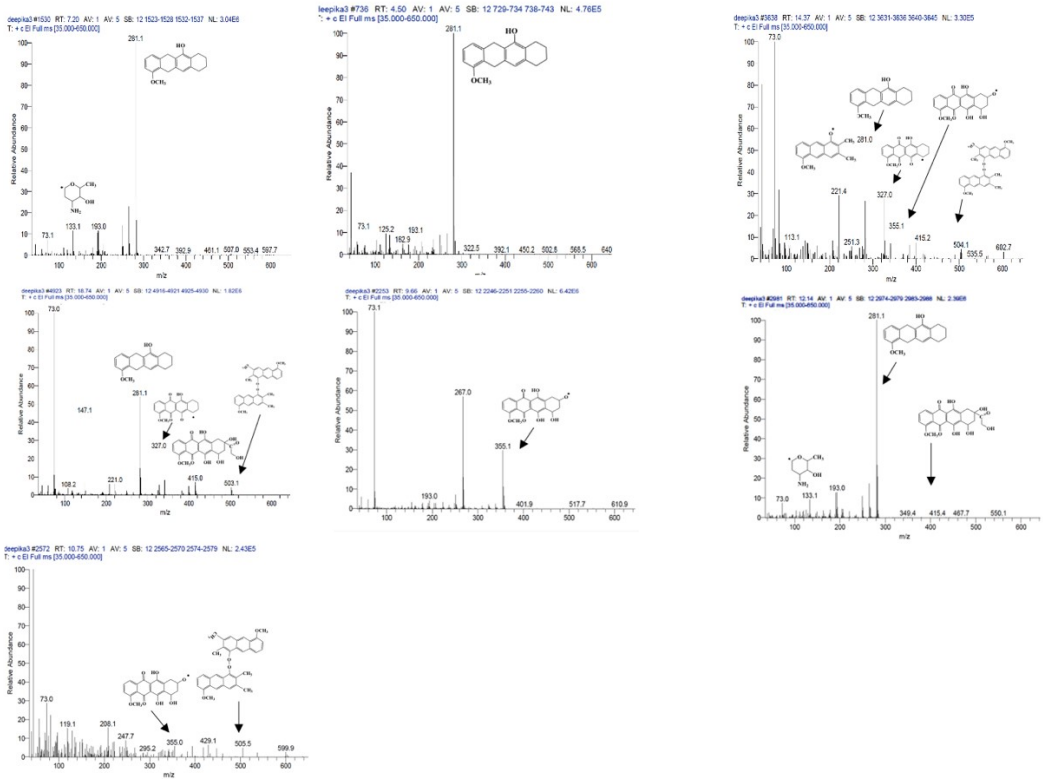

Fig. S13 GC-MS fragment analysis chart for DR degradation intermediates in presence of light only.

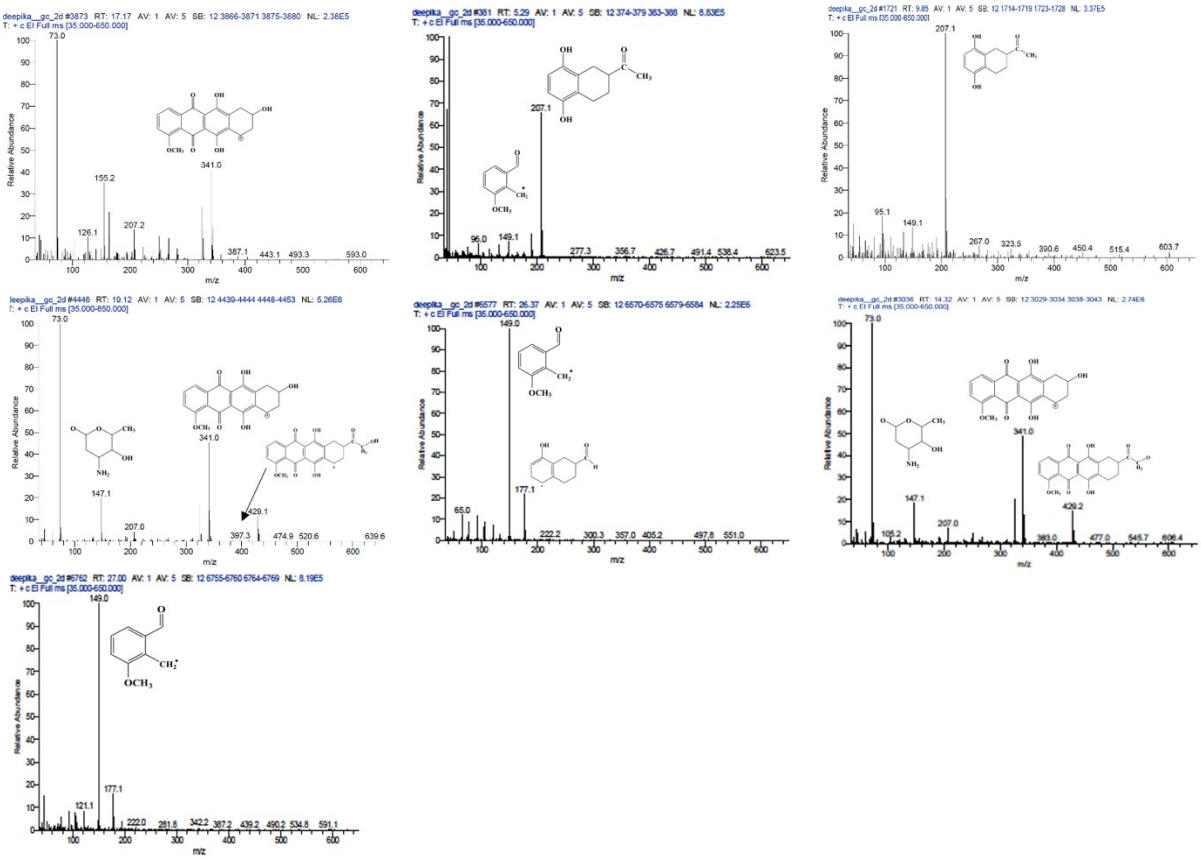

Fig. S14 GC-MS fragment analysis chart for DR degradation intermediates in presence of oxidant, BF 50AFTS and light.

Table S5 Possible intermediates of DR during degradation in presence of light only

DR After 7 h in light only	m/z	Structure
DR	545	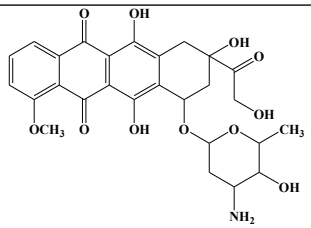
A1	414	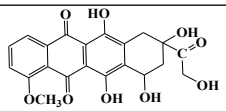

A2	355	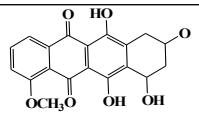
A3	327	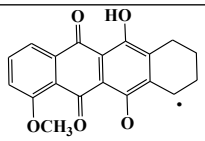 + 3H$^+$
A4	280	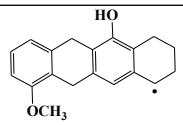 + H$^+$
A5	221	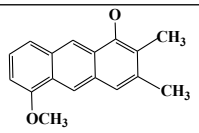
A6	502	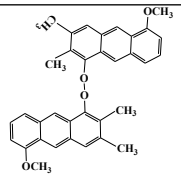 + 2H$^+$

316

317 **Table S6** Possible intermediates of DR during photocatalytic degradation (in presence of light,
318 H_2O_2 and BF 50AFTS at pH 2.5)

DR after 15 min	m/z	Structure
DR	545	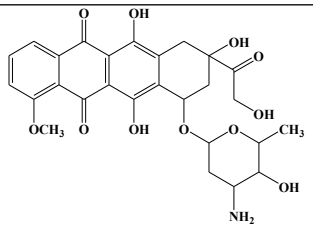
B1	397	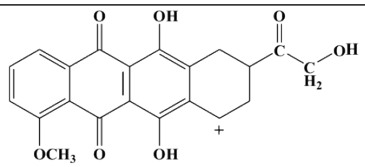
B3	383	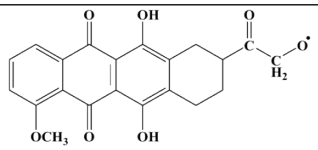

B4	341	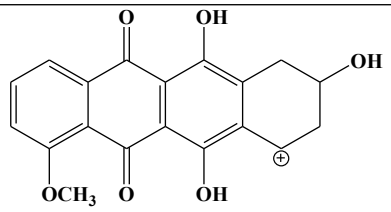
B6	207	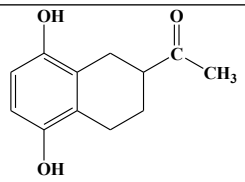
B2	147	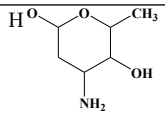
	73	4 H_2O + H^+
B8	177	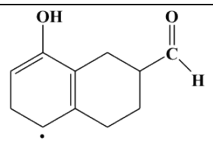
B7	149	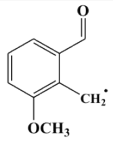
	65	2 H_2O + CO + H^+

Table S7 Toxicity assessment (using ECOSAR) of intermediates recorded during degradation of DR under different conditions.

DR After 7 h in light only	**Fish Toxicity (mg/L) LC_{50} (96 h)**	**DR after 15 min (catalyst + oxidant)**	**Fish Toxicity (mg/L) LC_{50} (96 h)**
DR	0.54	DR	0.54
A1	7.500	B3	1050
A2	0.200	B4	781
A3	0.040	B6	13.5

A4	0.087	B2	9480
A5	0.386	B8	11.1
A6	0.000034	B7	61.3

***Green highlights the reduction in toxicity as that of DR, whereas, Red highlights enhancement in toxicity.**

Table S8 MRI, GP% and calculated SVI values of *Vigna radiata* seed germination in contaminated river water (before and after phototreatment)

Pollutants added in river water	**MRE (cm) before phototreatment/ after phototreatment**	**GP% before phototreatment/after Phototreatment**	**SVI before phototreatment/after phototreatment**
DR	0.3/1.8	30/75	9/135
LF	1.8/2.2	70/90	126/198
For Controlled River water			
MRE (cm) in absence of BF 50AFTS/in presence of BF 50AFTS		**GP% in absence of BF 50AFTS/in presence of BF 50AFTS**	**SVI in absence of BF 50AFTS/in presence of BF 50AFTS**
2.5/2.8		95/95	237/266

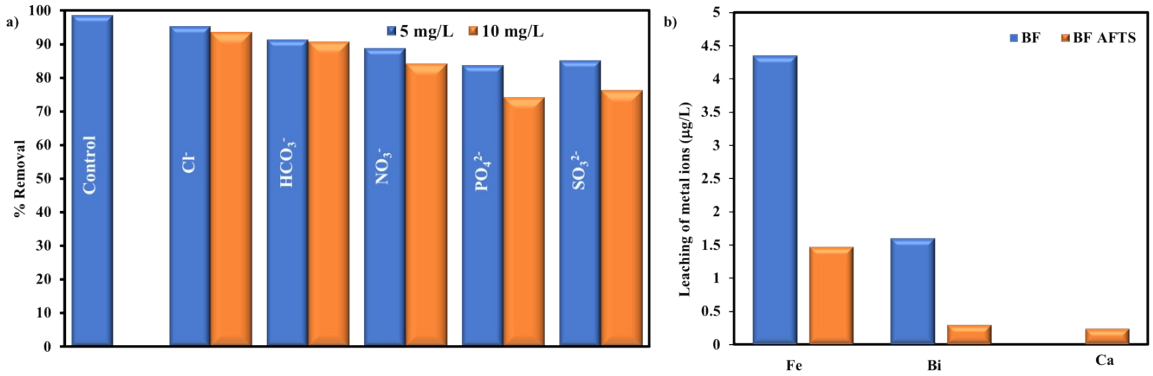

Fig. 15 (a) Interference of possible anions on %removal of DR (b) leaching of metal ions during degradation of DR utilizing BF an BF 50AFTS (catalyst amount used 0.60 g/L and pH = 2.5)

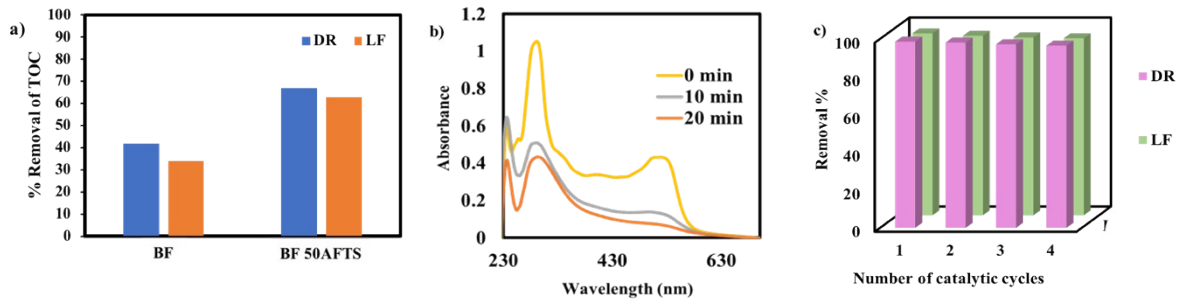

Fig. S16 (a) % Removal of TOC using BF and BF 50AFTS, (b) Time-dependent UV–visible spectra for degradation of mixture of SO, RB-Y, DR and LF using BF 50AFTS p-n/n homo-heterojunction , (c) Recyclability studies of BF 50AFTS.

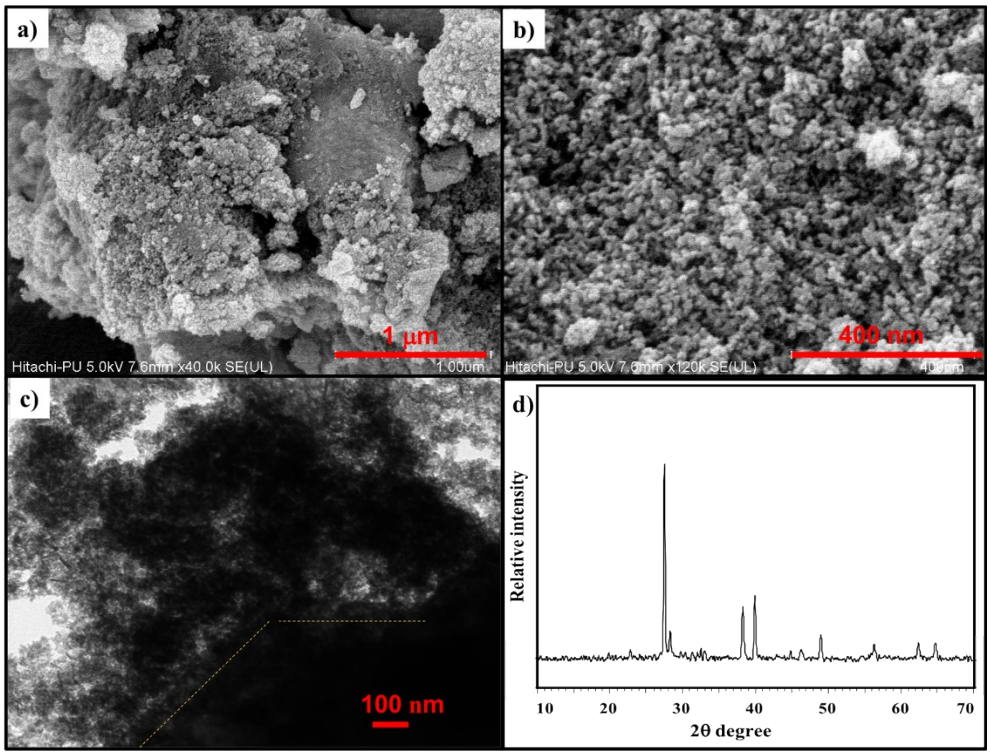

Fig. S17 (a, b) FE-SEM image of recovered BF 50AFTS at 1 µm and 400 nm, (c) TEM image of recovered BF 50AFTS at 100 nm and (d) PXRD pattern of recovered BF 50AFTS.

Electrochemical Optimization Parameters

To investigate the effect one parameter was varied at a time keeping others constant. The GCE was cleaned properly using α-alumina powder. A uniform dispersion of best catalyst (BF 50AFTS, 5 mg/mL) was prepared in aqueous medium, 4 µL suspension was robbed to drop cast on pre-washed GCE and allowed to dry naturally.

Effect of pH

The pH of supporting electrolyte plays a vital role in the process of electrochemical detection, in order to attain the optimum pH, experiments at varying pH values were performed keeping accumulation potential and accumulation time constant (17.27 μM of DR drug in 0.1 M acetate buffer, +0.4 V accumulation potential and 80 s accumulation time). NaOH/HCl was added to the supporting electrolyte to adjust pH in range of 3-8 . It was observed that with increase in pH from pH 3 to 5, current response for DR elevated significantly as shown in Fig. S18 (a). With further increase in pH values noticeable loss in current response was evidenced, which may be due to the electrostatic repulsion between positively charged surface of DR and positively charged modified electrode (BF 50AFTS@GCE).[12] Thus, further electrochemical experiments were performed with supporting electrolyte having optimal pH 5.

Effect of accumulation potential and accumulation time

In order to perceive best current response and to ensure maximum accumulation of analyte over electrode surface, optimization studies of accumulation potential were performed via analyzing the current response in potential range +0.2 V to +0.7 V (17.27 μM of DR drug in 0.1 M acetate buffer at pH= 5, 80 s accumulation time). Initially, the oxidation peak current was found to increase with increase in accumulation potential and maximum current response was observed at +0.4 V, further increase in accumulation potential resulted in declination of current response (Fig. S18 (b). Since, accumulation potential should be more negative to ensure the maximum deposition through reduction of the targeted analyte, hence, +0.4 V accumulation potential was chosen for further experimental studies.

Accumulation time is the specific time interval given to the ions (ions of DR present in electrolyte) to deposit on the surface of GCE at optimum accumulation potential. The square wave experiments were performed with varying accumulation time from 20 to 140 s (at pH= 5, Potential range +0.2 V to +0.7 V) and was observed that with elevation in accumulation time, current response for DR drug increased and get saturated at 80 s (Fig. S18 (c)). The saturation of current could be attributed to the formation of multilayer and saturation of electrode surface with reduced DR ions. Hence, +0.4 V accumulation potential for 80 s was chosen for further investigations of DR sensing.[13]

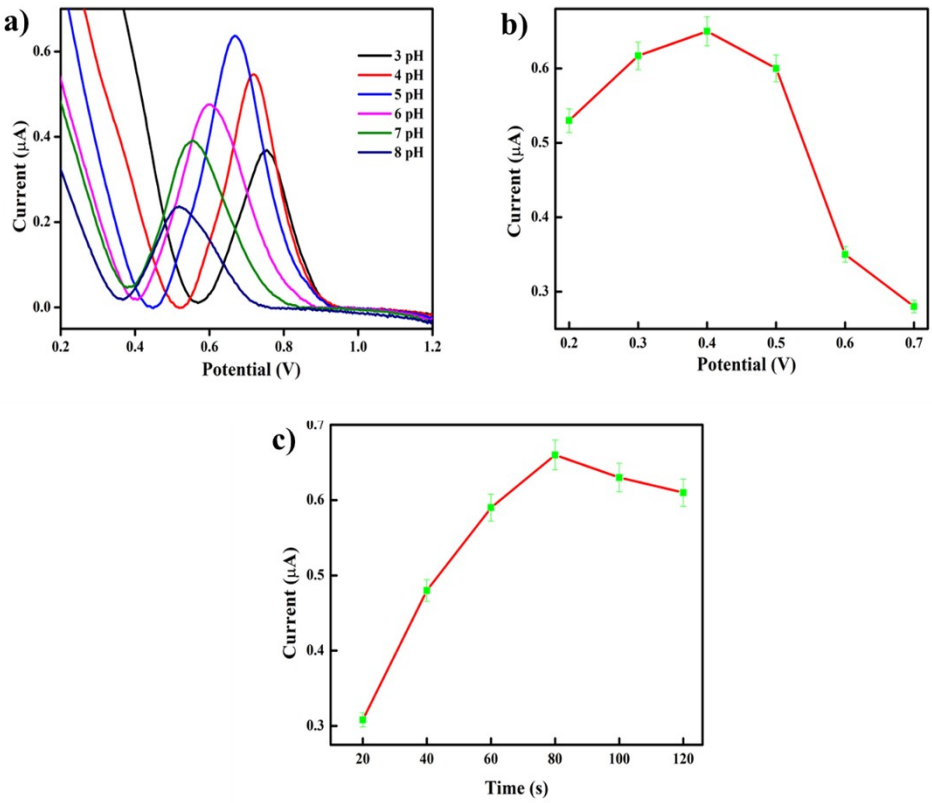

Fig. S18 SWASV response of BF 50AFTS@GCE for DR (a) at different pH in acetate buffer (b) with varying accumulation potential (c) for different accumulation times.

Interference, Repeatability and Reproducibility studies

Presence of other active species in real samples can interfere in the detection process and may mislead the analytical results. Thus, in order to investigate the anti-interference property of designed sensor, various interfering ions (drugs, uric acid, ascorbic acid, dopamine, glucose and aminophenols) were added to the electrolyte solution along with DR drug (17.27 μM of DR drug) under optimized conditions and the results are showcased in Fig. S19. Despite the introduction of high concentration (100 fold in comparison of analyte concentration) of interfering ions no significant effect on the obtained current response was observed, which clearly predicts that, co-existence of other active species in medium failed to alter the sensing ability of the designed sensor towards DR drug. The value of relative standard deviation (RSD) was found to be 2.60 %, thereby, results affirms the robustness of the design sensor which can easily detect the DR drug even in the presence of high concentration of interfering ions in the solution.

The designed sensor was testified upto 4 repetitive cycles of square wave voltammetric analysis for sensing of DR drug under optimized reaction conditions, no significant change in

current response was witnessed (Fig. S20 (a)). 0.62 % relative standard deviation was observed, whereas, 99% current was found to be retained even after 4 cycles. After repeatability, reproducibility experiments were performed by preparing 5 independent assembly of BF 50AFTS@GCE (under optimized conditions), the obtained results bespeaks 1.54 % RSD for 5 freshly modified electrodes (Fig. S20 (b)). Thus proffer sensor could be employed for long term prospective implementation.

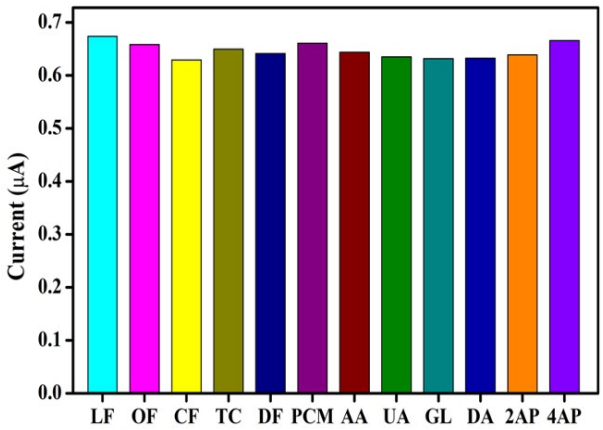

Fig. S19 Interference studies for various drugs (levofloxacin (LF), ofloxacin (OF), ciprofloxacin (CF), tetracycline (TC), diclofenac (DF), paracetamol (PCM)), ascorbic acid (AA), uric acid (UA), glucose (GL), dopamine (DA) and nitro phenols (2-aminophenol (2AP) and 4-aminophenol (2AP)) on detection of 17.27 μM of DR in 0.1 M acetate buffer (pH = 5.0)

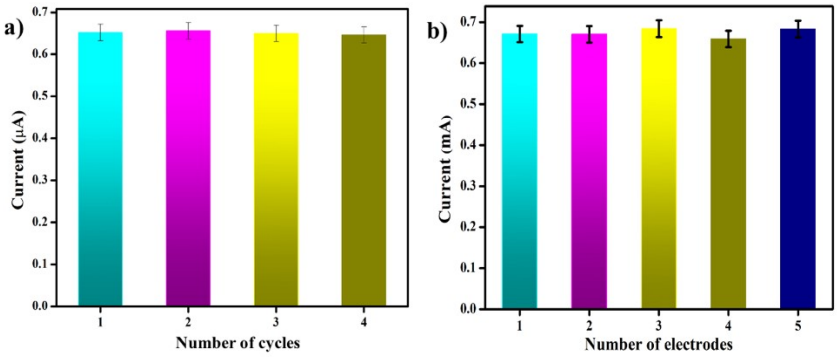

Fig. S20 (a) Current response obtained for 17.27 μM DR drug obtained from repeatability analysis of BF 50AFTS@GCE and (b) Reproducibility analysis of BF 50AFTS@GCE with 17.27 μM DR under optimized parameters.

Literature Comparison

Table S9 Comparison of present work with recently published $Bi_2Fe_4O_9$ based literature reports.

S.No	Material used	Application	Amount removed (time)	Phytotoxicity assessment	Exploration of by-Products/Use of light required	Mixture /industrial sample/ biowaste utilization	Year (Reference)
1	$BiFeO_3/Bi_2Fe_4O_9$	Methylene blue degradation	83% in 3 h	-	No/Yes	No/No/No	2022[14]
2	$Bi_2Fe_4O_9$	Bisphenol degradation	98.3% in 30 min	-	Yes/Yes	No/Yes/No	2022[15]
3	$BiFeO_3/Bi_2Fe_4O_9$	Methyl orange, Methylene blue, Rhodamine B, methyl red, acid red and Congo red dyes degradation	92, 82, 75, 70, 62, and 98% in 120 min	-	No/Yes	Yes/No/No	2021[16]
4	$Bi_2(1-x)Gd_2xFe_4O_9$	Methylene blue dye degradation	77% in 80 min	-	No/Yes	No	2021[17]
5	$Bi_2Fe_4O_9$	Tartrazine yellow dye degradation	99.34% in 120 min	-	No/Yes	No	2020[18]
6	$Bi_2Fe_4O_9$/ PMS	Sulfamethoxazole degradation	>95% in 30 min	-	Yes/Yes	No/Yes/No	2019[19]
7	g-C_3N_4/RGO/BFO	Congo Red dye degradation	86.7% in 60 min	-	No/Yes	No	2020[20]
8	g-C_3N_4/CNT/BFO	acid orange 7 degradation	85% in 4 h	-	No/Yes	No	2018[21]

9	$BiFeO_3/Bi_2Fe_4O_9/H_2O_2$	Sulfamethoxazole degradation	95% in 270 min	-	Yes/Yes	Yes/No/No	2020[22]
10	$BFO_{249}/rGO_{4.5}$	bisphenol A degradation	80% in 3 h	-	No/Yes	No	2015[23]
11	**BF AFTS**	**DR, LF drugs oxidative degradation; Electrochemical detection of DR drug**	**98.6% (in 12 min) and 96.3% (in 30 min); Limit of detection of DR (LOD) 1.99 nM**	**Yes**	**Yes/No**	**Yes/Yes/Yes**	**Present work**

References

[1] Mushtaq F, Chen X, Hoop M, Torlakcik H, Pellicer E, Sort J, Gattinoni C, Nelson BJ, Pané S. Piezoelectrically enhanced photocatalysis with $BiFeO_3$ nanostructures for efficient water remediation. I science. 2018 Jun 29;4:236-46.

[2] Komal, Gupta K, Kaur S, Kaur J, Kaushik A, Singhal S. A comparative analysis of source based distinctly functionalized nanostructured cellulose for the adsorptive removal of toxic colorants. Cellulose. 2019 Feb 15;26:1703-24.

[3] Kaur P, Singh S, Kumar V, Tikoo KB, Kaushik A, Singhal S. Development of emphatic catalysts for waste water remediation via synchronized free radical and non-free radical routes with composites of strontium hexaferrite, graphene and multi-walled carbon nanotubes. Ceramics International. 2022 Feb 15;48(4):4795-811.

[4] Mathew SS, Sunny NE, Shanmugam V. Green synthesis of anatase titanium dioxide nanoparticles using Cuminum cyminum seed extract; effect on Mung bean (Vigna radiata) seed germination. Inorganic Chemistry Communications. 2021 Apr 1;126:108485.

[5] Murshed MM, Nénert G, Burianek M, Robben L, Mühlberg M, Schneider H, Fischer RX, Gesing TM. Temperature-dependent structural studies of mullite-type $Bi_2Fe_4O_9$. Journal of Solid State Chemistry. 2013 Jan 1;197:370-8.

[6] Ashok B, Hariram N, Siengchin S, Rajulu AV. Modification of tamarind fruit shell powder with in situ generated copper nanoparticles by single step hydrothermal method. Journal of Bioresources and Bioproducts. 2020 Aug 1;5(3):180-5.

[7] Maheswari CU, Reddy KO, Muzenda E, Shukla M, Rajulu AV. Mechanical properties and chemical resistance of short tamarind fiber/unsaturated polyester composites: Influence of fiber modification and fiber content. International Journal of Polymer Analysis and Characterization. 2013 Oct 3;18(7):520-33.

[8] Sun H, Liu Y, Zhang Y, Lv L, Zhou J, Chen W. Synthesis of $Bi_2Fe_4O_9$/reduced graphene oxide composite by one-step hydrothermal method and its high photocatalytic performance. Journal of Materials Science: Materials in Electronics. 2014 Oct;25:4212-8.

[9] Liu P, Sun H, Liu X, Sui H, Zhang Y, Zhou D, Guo Q, Ruan Y. Enhanced photocatalytic performance of $Bi_2Fe_4O_9$/graphene via modifying graphene composite. Journal of the American Ceramic Society. 2017 Aug;100(8):3540-9.

[10] Wang X, Fan J, Qian F, Min Y. Magnetic $BiFeO_3$ grafted with MWCNT hybrids as advanced photocatalysts for removing organic contamination with a high concentration. RSC advances. 2016;6(55):49966-72.

[11] Gupta K, Kumar V, Tikoo KB, Kaushik A, Singhal S. Encrustation of cadmium sulfide nanoparticles into the matrix of biomass derived silanized cellulose nanofibers for adsorptive detoxification of pesticide and textile waste. Chemical Engineering Journal. 2020 Apr 1;385:123700.

[12] Dumitru R, Ianculescu A, Păcurariu C, Lupa L, Pop A, Vasile B, Surdu A, Manea F. $BiFeO_3$-synthesis, characterization and its photocatalytic activity towards doxorubicin degradation from water. Ceramics international. 2019 Feb 1;45(2):2789-802.

[13] Datir SR, Das M, Singh RP, Jain S. Hyaluronate tethered,“smart” multiwalled carbon nanotubes for tumor-targeted delivery of doxorubicin. Bioconjugate chemistry. 2012 Nov 21;23(11):2201-13.

[14] Taazayet WB, Zouari IM, Hosni N, Dkhil B, Mliki NT. Facile synthesis of pure $BiFeO_3$ and $Bi_2Fe_4O_9$ nanostructures with enhanced photocatalytic activity. Journal of Materials Science: Materials in Electronics. 2021:1-6.

[15] Su C, Li R, Li C, Wang W. Piezo-promoted regeneration of Fe^{2+} boosts peroxydisulfate activation by $Bi_2Fe_4O_9$ nanosheets. Applied Catalysis B: Environmental. 2022 Aug 5;310:121330.

[16] Tian L, Gao PA, Wang FG, Li XW, Li G. Study on Preparation of $BiFeO_3$/ $Bi_2Fe_4O_9$Composite Photocatalyst and Photocatalytic Degradation of Various Organic Dyes in Waste Water. Russian Journal of Physical Chemistry A. 2021 Jul;95:1495-504.

[17] Rao KS, Kamath SM, Kumar RR, Kavitha G, MeherAbhinav E, Shri SS, Induja S, Gopalakrishnan C. Delineating the photocatalytic properties of doped mullite $Bi_2Fe_4O_9$ by virtue of Gd3+ ions. Materials Letters. 2021 Aug 15;297:129960.

[18] Casanova Monteiro F, Caetano EH, de Jesus Cubas P, Pupin AV, Monteiro JF, Fujiwara ST. $Bi_2Fe_4O_9$ in pellet form is an alternative in the wastewater treatment process. Journal of Environmental Science and Health, Part A. 2020 May 11;55(6):677-85.

[19] Oh WD, Chang VW, Lim TT. A comprehensive performance evaluation of heterogeneous $Bi_2Fe_4O_9$/peroxymonosulfate system for sulfamethoxazole degradation. Environmental Science and Pollution Research. 2019 Jan 21;26:1026-35.

[20] Shekardasht MB, Givianrad MH, Gharbani P, Mirjafary Z, Mehrizad A. Preparation of a novel Z-scheme g-C_3N_4/RGO/ $Bi_2Fe_4O_9$ nanophotocatalyst for degradation of Congo Red dye under visible light. Diamond and Related Materials. 2020 Nov 1;109:108008.

[21] Di L, Yang H, Xian T, Chen X. Construction of Z-scheme g-C_3N_4/CNT/ $Bi_2Fe_4O_9$composites with improved simulated-sunlight photocatalytic activity for the dye degradation. Micromachines. 2018 Nov 22;9(12):613.

[22] Hu ZT, Liu JW, Zhao J, Ding Y, Jin Z, Chen J, Dai Q, Pan B, Chen Z, Chen J. Enhanced $BiFeO_3$/ $Bi_2Fe_4O_9$/H_2O_2 heterogeneous system for sulfamethoxazole decontamination: System optimization and degradation pathways. Journal of Colloid and Interface Science. 2020 Oct 1;577:54-65.

[23] Hu ZT, Liu J, Yan X, Oh WD, Lim TT. Low-temperature synthesis of graphene/$Bi_2Fe_4O_9$ composite for synergistic adsorption-photocatalytic degradation of hydrophobic pollutant under solar irradiation. Chemical Engineering Journal. 2015 Feb 15;262:1022-32.